Inorganic Chemistry

Article

pubs.acs.org/IC

Synthesis and Structure of Bismuth(III)-Containing Noncentrosymmetric Phosphates, $Cs_3KBi_2M_4(PO_4)_6Cl$ (M = Mn, Fe). Monoclinic (*Cc*) and Tetragonal ($P4_3$) Polymorphs Templated by Chlorine-Centered $Cl(Bi_2Cs)$ Acentric Units

J. Palmer West,[†] Dino Sulejmanovic,[†] Shiou-Jyh Hwu,*[,†] Jian He,[‡] Don VanDerveer,[†] and B. Keith Johnson[†]

[†]Department of Chemistry, Clemson University, Clemson, South Carolina 29634-0973, United States

[‡]Department of Physics and Astronomy, Clemson University, Clemson, South Carolina 29634-0978, United States

Supporting Information

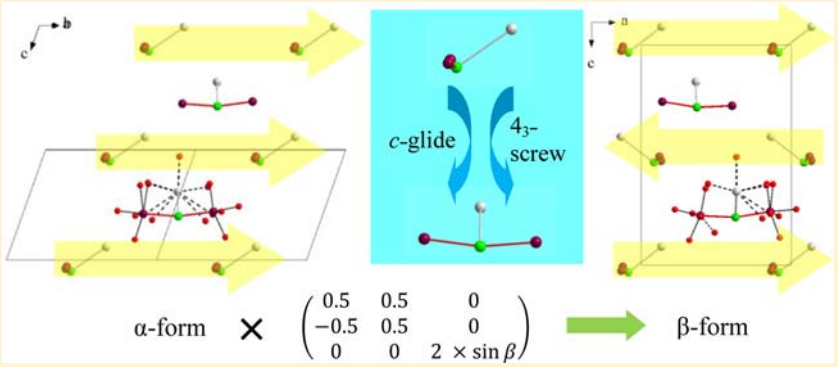

ABSTRACT: Single crystals of three new noncentrosymmetric (NCS) phosphates, α (**1**) and β (**2**) forms of $Cs_3KBi_2Mn_4(PO_4)_6Cl$ and α-$Cs_3KBi_2Fe_4(PO_4)_6Cl$ (**3**), were grown in a reactive CsCl/KCl molten-salt media. Their structures were determined by single-crystal X-ray diffraction methods showing that the α form crystallizes in the space group *Cc* (No. 9), which is in one of the 10 NCS polar crystal classes, *m* (2/*m*) while the β form crystallizes in $P4_3$ (No. 78) of another polar class, 4 (4/*m*). The unit cell parameters of the α form can be approximately correlated with that of the β form via the 3 × 3 orientation matrix [0.5, 0.5, 0; −0.5, 0.5, 0; 0, 0, 2 sin β]. The structures of these otherwise complicated phosphates exhibit two types of channels with circular and elliptical windows where the Cl-centered $Cl(Bi_2Cs)$ acentric unit is located. The neighboring acentric units are arranged in a parallel fashion in the α form, resulting in the monoclinic (*Cc*) lattice, but "antiparallel" in the β form, thus giving the tetragonal ($P4_3$) unit cell. **1**−**3** feature the compatible M−O−P unit that contains four crystallographically independent MO_x (x = 4, 5) polyhedra, which are connected to the $Cl(Bi_2Cs)$ acentric unit through one short and one long $M^{II}\cdots Cl$ bond. The compositions of **1** and **2** consist of three Mn^{2+} (d^5) and one Mn^{3+} (d^4) per formula unit and that of **3** has three Fe^{2+} (d^6) and one Fe^{3+} (d^5). Bond valence sums reveal that, in the α phase, the trivalent site adopts distorted tetrahedral $M(1)^{3+}O_4$ coordination and, in the β phase, distorted trigonal-bipyramidal $M(4)^{3+}O_5$. Thus far, the iron phase has only been isolated in the α form presumably because of little extra stabilization energy gain if the Fe^{2+} d^6 ion were to occupy the $M(1)O_4$ site. The possible origins pertaining to the structural differences in the α and β forms are discussed.

INTRODUCTION

Noncentrosymmetric (NCS) solids exhibit a variety of symmetry-dependent properties that include piezoelectricity, pyroelectricity, ferroelectricity, and second-order nonlinear-optical behavior.[1] A vast majority of NCS oxides, based on second-order Jahn−Teller (SOJT) cations, include the d^0 cations (e.g., Ti^{4+}, Nb^{5+}, W^{6+}, Mo^{6+}) and cations containing filled valence s shells (e.g., Sn^{2+}, Sb^{3+}, Pb^{2+}, Bi^{3+}, Se^{4+}, Te^{4+}).[2] We have been interested in the exploratory synthesis of salt-inclusion solids (SISs) in which we have discovered Cl-centered acentric units that serve as a template in the formation of special lattices, including NCS frameworks.[3] In our continued research, we incorporate SOJT ions, Bi^{3+} in this case, with the hope of enriching the formation of NCS framework solids in this already structurally versatile metal phosphate chemical system.

With respect to the synthesis of insulating magnetic oxides, our group is intrigued with employing closed-shell, non-magnetic, inorganic oxyanions as linkers (e.g., PO_4^{3-}) to structurally "encapsulate" magnetic nanostructures.[4] Upon using rigid, inorganic linkers in comparison to the organic

Received: May 15, 2012
Published: August 27, 2012

   dx.doi.org/10.1021/ic3010129 | *Inorg. Chem.* 2012, 51, 9723−9729

counterparts used in molecular solids, we hope to achieve magnetic behaviors similar to those at higher transition temperatures. We chose to incorporate bismuth also because Bi-containing oxide systems are well-known for their rich structural chemistry, especially for metastable states and polymorphs of ferroelectric interest.[5,6]

The occurrence of multiferroism is favored for polar NCS phases containing both magnetic and SOJT ions. In $BiMO_3$ (M = Cr, Mn, Fe), for instance, a $6s^2$ lone pair of Bi^{3+} is stereochemically responsible for the observed ferroelectric ordering, while the spin-polarized d electrons are responsible for magnetic ordering.[7−9] The perovskite-like phases having B-site cations responsible for both spontaneous polarization and magnetization are scarce because the transition-metal d electrons required for the spontaneous magnetization often destabilize the off-center ferroelectric distortion.[10] As a result, it is practically advantageous to incorporate ions, like Bi^{3+}, in conjunction with paramagnetic B-site cations.

In this paper, we present three new NCS phases comprised of mixed-valent (II and III), mid-row, transition-metal cations and SOJT Bi^{3+} ions, i.e., α-$Cs_3KBi_2Mn_4(PO_4)_6Cl$ (**1**), β-$Cs_3KBi_2Mn_4(PO_4)_6Cl$ (**2**), and α-$Cs_3KBi_2Fe_4(PO_4)_6Cl$ (**3**). So far, α and β polymorphs have been found for M = Mn, whereas only the α form has been found for M = Fe. Thus, we especially focus our discussions on the syntheses and structure characterizations with respect to the formation of different isomorphs. These compounds were isolated in reactive CsCl/KCl molten-salt media where salt inclusion is evident and a fascinating acentric $Cl(Bi_2Cs)$ unit is found to serve as a template responsible for the formation of the different polymorphs and, in turn, the bulk acentricity. In addition, the unexpected switching of the trivalent M^{3+} sites discovered in the two Mn-based polymorphs and the electronic factors possibly governing the missing β-Fe phase will be discussed in terms of the crystal-field stabilization energy (CFSE).

EXPERIMENTAL SECTION

All single-crystal growth reactions were loaded into a nitrogen-purged drybox, and reactants were placed in carbon-coated, fused silica ampules that were then flame-sealed under vacuum. It should be noted that the single-crystal syntheses below were originally set up to explore Bi−M−P−O phases and the CsCl/KCl salt was employed as a high-temperature solvent for crystal growth. Product yields are estimated visually based on the physical sizes of the crystalline phases obtained from representative portions of the total product after the unreacted flux was washed away.

Single-Crystal Growth of the Manganese Derivatives. The α polymorph was initially discovered as a minor product in a relatively Bi_2O_3-rich reaction. In the reaction, Bi_2O_3, Mn_2O_3, and P_4O_{10} were mixed in a 1:1:1 mole ratio (ca. 0.25 g) and added to a CsCl/KCl eutectic flux equal to 3 times the mass of the oxide reactants. The mixture was heated to 800 °C, held there for 4 days, slowly cooled to 400 °C (0.1 °C/min), and then furnace-cooled to room temperature. After washing with water to remove excess flux, dark-blue single crystals of **1** with multifaceted, chunky-shaped morphologies were retrieved in a yield of ∼30% [see Figure S1 in the Supporting Information for powder X-ray diffraction (PXRD) of selected crystals in question showing exclusively **1**, α]. Other products were red columns identified as members of the salt·$A_2Mn_3(P_2O_7)_2$ family, also known as CU-2 SIS[11] (∼50%), and an unidentified polycrystalline pink powder. Worth noting is the fact that, on the basis of the structural composition of **1**, there are formally three Mn^{2+} and only one Mn^{3+} ions per formula unit. The existence of the Mn^{2+} ion is likely because of the reduction of trivalent Mn_2O_3 by the carbon coating, which is, in turn, oxidized to CO_2/CO. A popping noise was heard when the ampules were cracked open, suggestive of a buildup of pressure possibly because of the CO_2/CO gas(es).

Single crystals of **2** (β) belong to the only polymorph discovered in a reaction using Bi_2O_3, Mn_2O_3, and P_4O_{10} in a 2:1:1 (ca. 0.25 g) mole ratio, different from that employed for the formation of **1** (α). The mixture was heated in the CsCl/KCl reactive flux under the same conditions as those of **1**. The shape and color for the crystals of **2** resemble those of **1**; however, the yield (∼10%) and crystal size are much smaller. Transparent chunk crystals, $Bi_{6.67}P_4O_{20}$[12] (∼70%), were also formed with an unidentified white powder. Because PXRD failed to conclude the coexistence of **1** and **2**, owing to an extremely low yield in this particular reaction, five randomly selected crystals were pooled for single-crystal X-ray diffraction (SXRD) studies and all were indexed as phase **2**.

In light of the results of the SXRD studies mentioned above, a stoichiometric molar ratio, with respect to the cations, was employed, i.e., 2:4:3 of Bi_2O_3, Mn_2O_3, and P_4O_{10}. Upon using the same flux and same conditions as those previously described, **1** and **2** were found to coexist. The product distribution of this particular reaction resembled that for the single-crystal growth of **1** except with a mixture of the dark-blue phases of **1** and **2**. Similarly, a stoichiometric attempt reaction accounting for Mn^{2+} and Mn^{3+} was employed using the following molar ratio: 2:6:1:3 of Bi_2O_3, MnO, Mn_2O_3, and P_4O_{10}. Neither **1** nor **2** was observed in this particular reaction, suggesting that the reduction of Mn_2O_3 by carbon coating possibly plays a crucial role.

Single-Crystal Growth of the Iron Derivative. Under the same exact conditions as those used for the growth of **1** and **2**, single crystals of **3** (α) were discovered in reactions using both 2:1:1 and 1:1:1 molar ratios of the reactants. Byproducts similar to those in the synthesis of **2** were observed, whereas yields of **3** and crystal sizes were similar to those in the synthesis of **1**. There is no experimental evidence of the β-form, Fe-containing isomorph as witnessed by PXRD of selected crystals from the reaction (Figure S2 in the Supporting Information). Also, the noticeable loss of carbon coating is suggestive of the reduction of iron oxide. Similar flux reactions were also performed whereby stoichiometric amounts of reactants were used. The SXRD analysis of these reactions only showed the presence of **3** (α) and not the β form. A minor impurity phase, brown sheetlike crystals of $CsFeSi_2O_6$, was also identified because of the chemical attack of quartz tubing.

Note that, in the Supporting Information, more information on stoichiometric synthetic attempts is given along with mention of the variable heating treatment of the 1:1:1 reaction that formed **1**.

Differential Scanning Calorimetry/Thermogravimetric Analysis (DSC/TGA). DSC/TGA measurements on a ground powder of selected crystals of **1** (∼25 mg) were done using a SDT Q600 TA Instruments calorimeter. A 110 μL platinum sample and reference pans were used for data collection. The heating profile for the measurement included a heating rate of 10 °C/min from room temperature to 1000 °C, followed by a return cooling rate of 10 °C/min in the presence of 75 mL/min nitrogen gas flow.

Structure Determination. For single-crystal structure studies, small-size chunky crystals of **1**−**3** were selected because crystals having multifaceted morphologies were twinned. For **1** and **2**, the crystals were dark blue, and for **3**, they were dark brown. Single crystals of **1**−**3** were selected under an optical microscope equipped with a polarizing light attachment. The data crystals were mounted on glass fibers with epoxy for X-ray diffraction studies. The data were collected at room temperature on a four-circle Rigaku AFC8 diffractometer equipped with a Mercury CCD area detector, with Mo Kα (λ = 0.71073 Å) radiation. An empirical multiscan absorption correction was applied using *REQAB*,[13] a subroutine of the *CrystalClear*[14] software package. Refinement of the crystal structures of **1**−**3** using a full-matrix, least-squares technique via the *SHELXTL* packaging software (version 6.1) was performed.[15] **1** and **3** crystallize in a monoclinic crystal system with the polar space group *Cc* (No. 9). The refinement of **1** yielded a Flack parameter of 0.25(1) with 78.8% Friedel coverage and an R1 of 0.0578, indicating that the crystal was composed of a racemic twin. Refinement using the TWIN and BASF commands in *SHELXTL*

dx.doi.org/10.1021/ic3010129 | *Inorg. Chem.* 2012, 51, 9723−9729

Table 1. Crystallographic Data for $Cs_3KBi_2M_4(PO_4)_6Cl$, Where M = $Fe^{2+/3+}$ and $Mn^{2+/3+}$

empirical formula	α-$Cs_3KBi_2Mn_4(PO_4)_6Cl$ (**1**)	β-$Cs_3KBi_2Mn_4(PO_4)_6Cl$ (**2**)	α-$Cs_3KBi_2Fe_4(PO_4)_6Cl$ (**3**)
fw	1680.82	1680.82	1684.46
cryst syst	monoclinic	tetragonal	monoclinic
cryst dimens, mm	0.18 × 0.16 × 0.10	0.22 × 0.19 × 0.14	0.20 × 0.18 × 0.08
cryst color/shape	dark blue/chunks	dark blue/chunks	dark brown/chunks
space group, *Z*	*Cc* (No. 9), 4	$P4_3$ (No. 78), 4	*Cc* (No. 9), 4
T, °C	27	27	27
a, Å	17.362(4)	12.210(2)	17.167(3)
b, Å	17.138(3)	12.210(2)	17.089(3)
c, Å	9.993(2)	17.848(4)	9.928(2)
β, deg	116.91(3)		116.66(3)
V, Å^3	2651.4(9)	2660.7(8)	2602.8(9)
μ(Mo Kα), mm^{-1}	19.852	19.782	20.512
d_{calc}, g/cm^3	4.211	4.196	4.299
data/restraints/param	4220/2/346	4689/1/345	4040/2/346
final R1/wR2[a] [$I > 2\sigma(I)$]/GOF	0.0511/0.1240/1.063	0.0528/0.1335/1.119	0.0482/0.1171/1.099
Flack parameter/Friedel coverage (%)	0.291(9)/78.8	−0.013(8)/93.0	0.205(8)/75.3
largest diff peak/hole, e/Å^3	2.505/−2.469	3.034/−2.026	3.560/−2.628

[a]For **1**, R1 = $\sum||F_o| - |F_c||/\sum|F_o|$, wR2 = $[\sum w(|F_o| - |F_c|)^2/\sum w|F_o|^2]^{1/2}$, and $w = 1/[\sigma^2(F_o^2) + (0.0657P)^2 + 0.0000P]$, where $P = (F_o^2 + 2F_c^2)/3$. For **2**, R1 = $\sum||F_o| - |F_c||/\sum|F_o|$, wR2 = $[\sum w(|F_o| - |F_c|)^2/\sum w|F_o|^2]^{1/2}$, and $w = 1/[\sigma^2(F_o^2) + (0.0672P)^2 + 11.0070P]$, where $P = (F_o^2 + 2F_c^2)/3$. For **3**, R1 = $\sum||F_o| - |F_c||/\sum|F_o|$, wR2 = $[\sum w(|F_o| - |F_c|)^2/\sum w|F_o|^2]^{1/2}$, and $w = 1/[\sigma^2(F_o^2) + (0.0606P)^2 + 47.4873P]$, where $P = (F_o^2 + 2F_c^2)/3$.

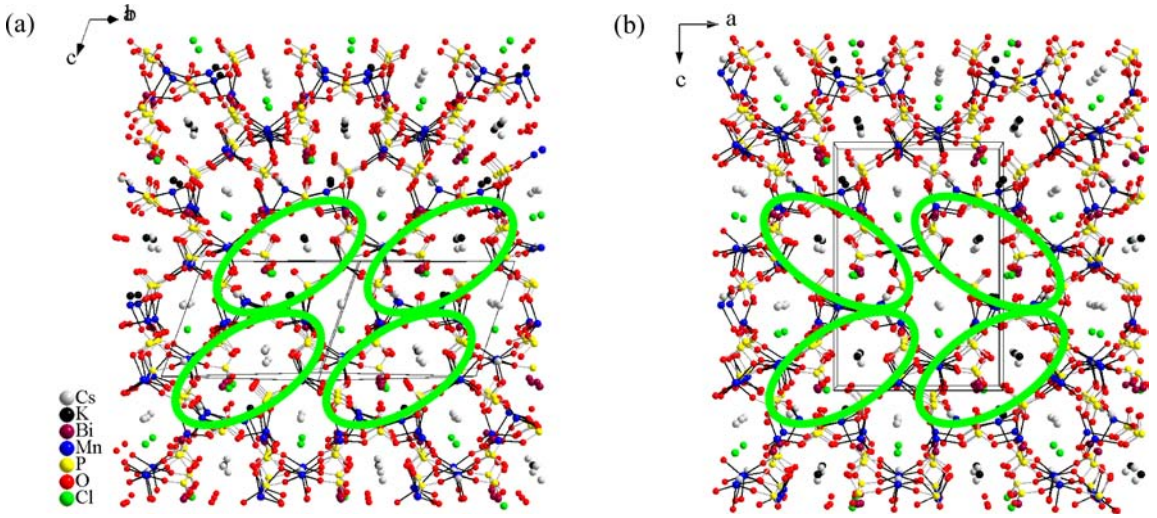

Figure 1. Perspective views of the $Cs_3KBi_2Mn_4(PO_4)_6Cl$ structure crystallizing in space groups *Cc* (a) along [−1, 1, 0] and $P4_3$ (b) along [0, 1, 0]. A structural comparison of the two isomorphs is highlighted by orientation of the open-framework windows in green circles; see the text.

resulted in a slight statistical improvement of R1 to 0.0511. Similarly, with the refinement of **3**, the residuals were R1 = 0.0525 with a Flack parameter of 0.184(8) and Friedel coverage of 75.3%. Upon the same treatment as **1** with the TWIN and BASF commands, R1 was improved to 0.0482.

2 crystallizes in a tetragonal crystal system with the polar, as well as chiral, space group $P4_3$ (No. 78). During the final stages of refinement of **2**, the Flack parameter was determined to be −0.013(8), with 93.0% Friedel coverage and an R1 of 0.0528.

The refinements of **1**−**3** led to a few O atoms with large and distorted thermal parameters. Data recollected at lower temperatures (−160 °C) for **1** did not show an overall improvement in the number of O atoms with large *U*(eq). Also, disorder for these specific O atoms was not modeled in the final structure solution because refinements did not show any partial occupancy. Potential problems associated with the space-group assignment of **1**−**3** were checked using *PLATON*,[16] and no higher symmetry was suggested.

In order to further confirm the NCS assignments of **1**−**3**, attempts were made to solve **1** in the corresponding centrosymmetric space group *C*2/*c* (No. 15) and to solve **2** in $P\bar{4}$ (No. 81), $P4/m$ (No. 83), and $P4_2/m$ (No. 84), all of which yielded unreasonable refinements. In addition, the preliminary second harmonic generation (SHG) efficiency of **1** was evaluated using the reported methods.[1g] The observation of green light along with the acquisition of an SHG efficiency approximately equal to α-SiO_2 confirmed the NCS space group.

A summary of the crystallographic data of **1**−**3** can be found in Table 1, and selected bond distances and angles are listed in Tables S1 (for **1** and **2**) and S2 (for **3**) in the Supporting Information.

RESULTS AND DISCUSSION

Synthesis. As stated before, we began exploratory synthesis in a relatively Bi-rich region of the chemical system where isolation of new Bi-containing phases can more likely be ensured. Two sets of reactions with molar ratios of the corresponding binary oxides of 1:1:1 and 2:1:1 were first employed, from which three new NCS phases were synthesized in two different polymorphs. The results showed that the α (**1**) and β (**2**) Mn-containing phases were isolated exclusively from

dx.doi.org/10.1021/ic3010129 | *Inorg. Chem.* 2012, 51, 9723−9729

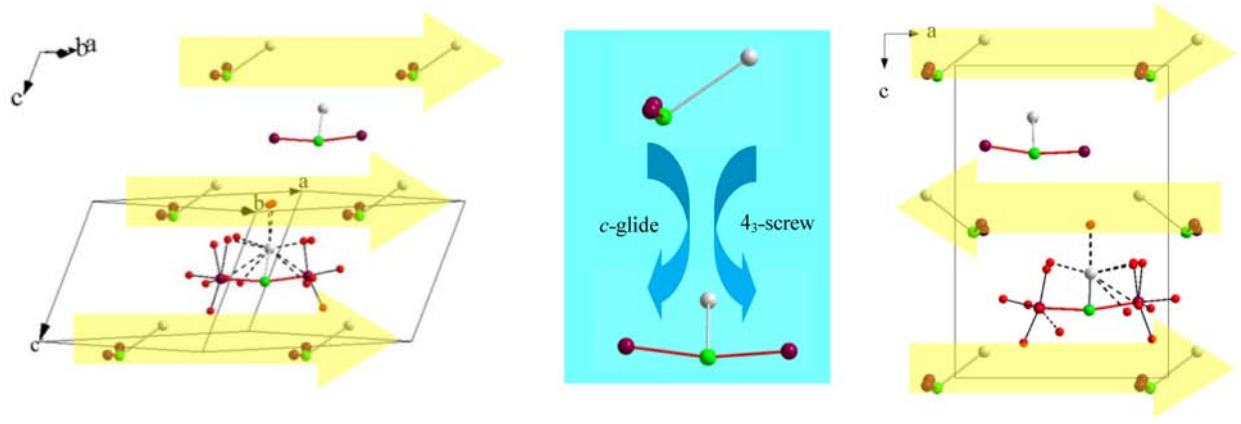

Figure 2. $Cl(Bi_2Cs)$ unit residing in the elliptical channels in **1** (a) and **2** (c). Coordination around Bi and Cs is highlighted in one unit for clarity. The symmetry correlation of the neighboring rows of the $ClBi_2Cs$ units is highlighted (b). One unique set of dipoles in the (0, 0, 2) planes is indicated by yellow arrows; see the text. Color code: Cl, green; Cs, gray; Bi, purple; O, red.

their respective reaction mixtures, while the coexistence of the two was observed, as expected, in the reaction with a stoichiometric ratio of Bi:Mn:P. The α form (**3**) is the only Fe-containing polymorph discovered thus far independent of using either molar ratio of Bi:Fe:P. This could be, in part, due to the difference in the structures of Fe_2O_3 and Mn_2O_3 and their respective melting points, i.e., 1539 versus 1080 °C (dec), and thus different reactivities.[17] It is also realized that, oftentimes, differences between the formations of Mn- and Fe-containing derivatives are caused by preferred CFSEs relative to the particular crystal site adopted by these Jahn–Teller Mn^{3+} d^4 and Fe^{2+} d^6 ions; see below. A notable example of such behavior is observed in the spinel versus inverse-spinel compounds.[18]

Structure Description. $Cs_3KBi_2Mn_4(PO_4)_6Cl$ exists in two polymorphs, namely, α (**1**) and β (**2**), corresponding to the monoclinic (Cc) and tetragonal ($P4_3$) phases, respectively, and $Cs_3KBi_2Fe_4(PO_4)_6Cl$ exists solely in one, the α form (**3**). Structural analysis of these otherwise structurally complex oxides revealed that the cell dimensions of the two polymorphs in general can be related by $(a, b, c)_\beta = [0.5, 0.5, 0; -0.5, 0.5, 0; 0, 0, 2 \sin \beta](a, b, c)_\alpha$. Given this correlation, we drew the perspective views of the α and β Mn-containing derivatives along [−1, 1, 0] and [0, 1, 0], respectively, in order to better compare the two polymorphs (Figure 1).

Structural analysis reveals that the 3D frameworks consist of pseudo-1D channels with circular- and elliptical-shaped windows. The latter is highlighted in green circles. In the α phase (Figure 1a), the elliptical-shaped windows are shown to be stacked "parallel" to one another along [0, 0, 1], whereas in the β phase, these windows are shown to be stacked "antiparallel". The stacking in the α phase is slanted along c; thus, the related dimension with respect to β can be expressed by a factor of 2 sin β.

Detailed structural analysis reveals the existence of a Cl-centered $Cl(Bi_2Cs)$ acentric unit residing in the channels with elliptical windows. The respective formation of these two polymorphic NCS structures can be simply discerned by the symmetry correlations of the neighboring $Cl(Bi_2Cs)$ units, as shown in Figure 2. The orientations of the stacked $Cl(Bi_2Cs)$ acentric units along [0, 0, 1] are related by the c-glide symmetry operator for the α phase and the 4_3 screw for the β phase (Figure 2b). [For clarity, additional views of the $Cl(Bi_2Cs)$ units are given in Figure S6 in the Supporting Information showing the relative positions of these symmetry operators in their respective unit cells.] The acentric units with the same orientations reside in every other row. The immediate neighboring rows of acentric units form in an orthogonal direction to each other and so do the corresponding elliptical channels where they reside. It is thus evident that the orientation of these acentric units, like a template, dictates the relative orientations of the elliptical windows seen in Figure 1 and the nonintercepting, orthogonal channels.

In addition, for the structure of the β phase (Figure 2c), the dipoles in the (0, 0, 2) planes, as indicated by yellow arrows, are presumably canceled because of the antiparallel arrangement of the acentric $Cl(Bi_2Cs)$ units along the [1, 0, 0] and [0, 1, 0] directions. So, the net dipole and thus the polarity is, as expected, along c. Nonetheless, the Cl-centered $Cl(Bi_2Cs)$ acentric unit does indeed provide an effective way for structural analysis as well as a description for the bulk acentricity of these otherwise extremely complicated framework structures.

It is also realized that the α and β forms are made of the same M–O–P unit consisting of four crystallographically distinct MO_x (x = 4, 5) polyhedral units, two of which, i.e., Mn(2) and Mn(3) in **1** and **2**, are connected to the $Cl(Bi_2Cs)$ units through one short and one long Mn···Cl bond, as shown by the dotted lines in Figure 3a,b. It is noted that transition-metal phosphate frameworks are known for their versatility. Through $P(4,5)O_4$ tetrahedra (Figure 3b), the asymmetric M–O–P units are shown to be interconnected in one of two different ways to accommodate the parallel versus antiparallel orientations of the acentric $Cl(Bi_2Cs)$ units observed in the α and β polymorphs, respectively. The connectivity of the M–O–P framework is illustrated further in Figure S7 in the Supporting Information with respect to elliptical windows of different orientations. Meanwhile, three of the four crystallographically independent MO_x polyhedra form the M_3O_{12} trimer consisting of edge-shared $M(2,3)O_5$ and vertex-shared $M(4)O_5$. Each trimer is interlinked with the isolated $M(1)O_4$ tetrahedron via $P(2,6)O_4$ units (Figure 3a).

Not only do the Cl atoms play a structural role in the formation of acentric $Cl(Bi_2Cs)$ units, they saturate the coordination geometry around the corresponding transition-metal cations, M^{2+}. The coordination of two edge-shared polyhedra in the trimer unit is thus expanded from [5], in MO_5, to [5 + 1], in MO_5Cl, because of the Cl atoms of the neighboring acentric $Cl(Bi_2Cs)$ unit. The structure of the

dx.doi.org/10.1021/ic3010129 | Inorg. Chem. 2012, 51, 9723–9729

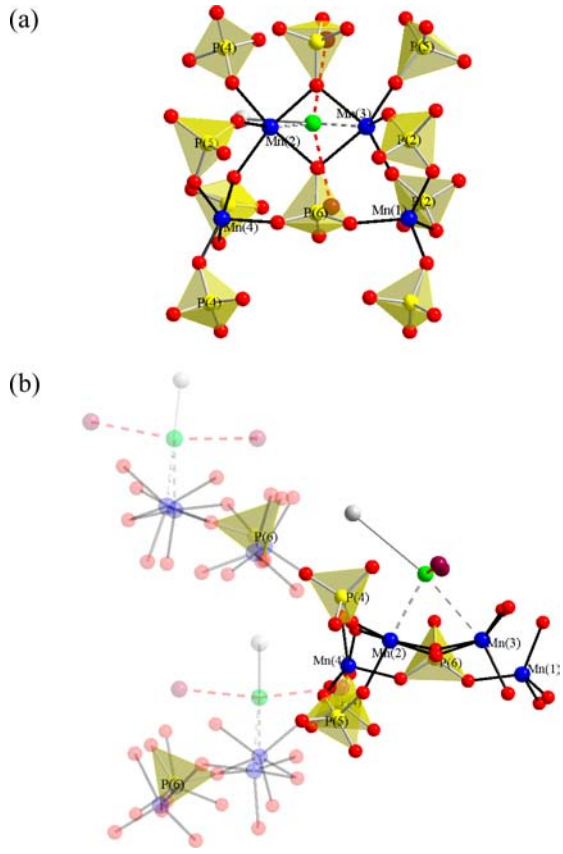

Figure 3. (a) Partial structure of **2** (β form) representatively showing one asymmetric unit of four transition-metal atoms, Mn_4 in this case, capped by PO_4 units (drawn in yellow tetrahedra) and its connection with the $Cl(Bi_2Cs)$ unit. (b) Partial structure showing the connectivity of three neighboring Mn_4 units via inter-$P(4,5)O_4$ groups.

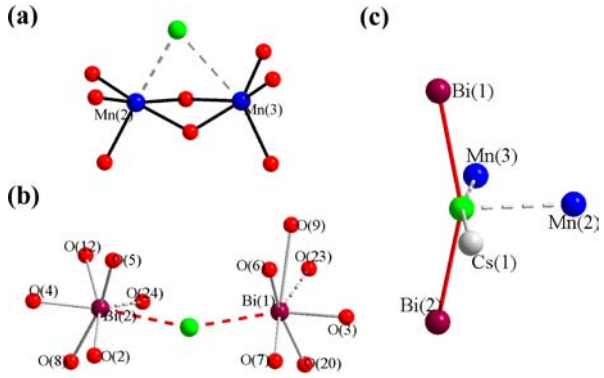

Figure 4. (a) Face-shared MnO_5Cl distorted [5 + 1] octahedra and (b) connectivity of two BiO_6Cl polyhedra in **2** showing (c) the structural role of Cl; see the text.

trimer unit in **2** thus consists of two distorted $Mn(2,3)O_5Cl$ [5 + 1] octahedra sharing triangular faces (Figure 4a) to give rise to a $[Mn_2O_8Cl]$ dimer. The Mn···Cl interactions are relatively inhomogeneous judging from the asymmetric bond distances, 2.72(1) and 3.13(1) Å (Table S1 in the Supporting Information), with respect to the sum of the Shannon crystal radii,[19] 2.74 Å, of a six-coordinate Mn^{2+} cation, 0.970 Å (high spin, HS), and Cl^-, 1.67 Å. In addition, this unique Cl atom is also shared by two Bi atoms of BiO_6Cl (Figure 4b). So, a complete description of the coordination around Cl, as depicted in Figure 4c, is square-pyramidal (sq py) $Cl(Bi_2CsMn_2)$, with Mn(2) being the vertex atom. The basal plane is slightly distorted from an ideal square-planar geometry as the sum of the orthogonal angles is 363.7°. The angles to the vertex Mn(2) are quite diverse: 68.1° for Mn(3), 96.9° for Bi(2), 102.2° for Bi(1), and 102.3° for Cs(1). This is presumably due to the structural strain of the $[Mn(2,3)_2O_8Cl]$ dimer.

The $Bi_2O_{12}Cl$ unit shown in Figure 4b is made of two BiO_6Cl polyhedra with little definition in geometry. For the $Bi(1)O_6Cl$ unit, the Bi(1)−O bond distances range from 2.14 to 2.73 Å and from 2.11 to 2.88 Å (Table S1 in the Supporting Information) in the α and β forms, respectively. The average Bi(1)−O bond distances are 2.45 and 2.44 Å, which are both a little longer than the expected sum of the Shannon radii[19] (2.38 Å) of a six-coordinate Bi^{3+}−O species. A Cl^- ion is bound to one of the apexes with Bi(1)−Cl bond distances of 2.885(7) and 2.894(6) Å. This Cl atom is shared with the other Bi atom, Bi(2), in a distorted $Bi(2)O_6Cl$ polyhedron. Comparable to Bi(1), the Bi(2)−O bond distances range from 2.15 to 3.24 Å and from 2.18 to 2.94 Å with average Bi(2)−O bond distances of 2.48 and 2.44 Å, while the Bi(2)−Cl bond distances are 2.898(7) and 2.909(5) Å.

Surprisingly, the bond valence sum (BVS) calculations[20] (Table S3 in the Supporting Information) indicate that the trivalent M^{3+} site alternates between the α and β forms. The trivalent cation resides in the isolated $M(1)O_4$ tetrahedral site in α as expected because the size of the M^{3+} ion is smaller than that of M^{2+}. In β, it resides in one of the trimer sites centered in the trigonal-bipyramidal (tbp) $M(4)O_5$. Given the crystal-field splitting of $(x^2 - y^2, z^2)(xy, yz, xz)$ for the tetrahedral coordination as opposed to $(xz, yz)(x^2 - y^2, xy)(z^2)$ for the tbp coordination, the HS Mn^{3+} d^4 ion may not post much overall gain in the stabilization energy through the tbp distortion such as that observed in β; thus, the population of Mn^{3+} in either site makes it possible to accommodate the structural distortion of the overall M−O−P framework. Assuming a HS electronic configuration, the sole observation of the α-Fe form may be rationalized as follows. For Fe^{3+}, a d^5 non-Jahn−Teller ion, no gain of the stabilization energy is thus expected by occupation of either the tetrahedral or tbp sites. However, for a HS Fe^{2+} d^6 ion, we speculate that the CFSE would be too little to compensate for the inherent repulsive interaction between oxide anions in the smaller tetrahedral site than tbp, thus the sole observation of the α phase. Nevertheless, M−O bond distances, as well as M−Cl, for tetrahedral $M(1)O_4$, pseudo[5 + 1]-octahedral $M(2,3)O_5Cl$, and tbp $M(4)O_5$ are all comparable with those observed in the previously reported Cl-containing NCS phases.[3] The oxidation-state distributions are Bi^{3+}, $Mn/Fe(1)^{3+}$, and $Mn/Fe(2-4)^{2+}$ in the α form and Bi^{3+}, $Mn(1-3)^{2+}$, and $Mn(4)^{3+}$ in the β form.

DSC/TGA. DSC/TGA was performed on ground powder of selected crystals of **1**, as seen in Figure 5. On the basis of the DSC measurements, there appear to be two endothermic peaks, each corresponding to the onset temperatures of ~695 and ~745 °C. Both of these endothermic peaks are believed to be associated with two definite decompositions, as is evident by the percent weight losses in TGA of ~2.2 and ~4.5%. We speculate that the initial decomposition could be due to the evaporation of chlorine, which amounts to a 2.1% theoretical weight loss. The remaining decomposition corresponding to further weight loss seems to have a continuous and albeit gradual decrease to 1000 °C. In fact, it is difficult to assign the

dx.doi.org/10.1021/ic3010129 | Inorg. Chem. 2012, 51, 9723−9729

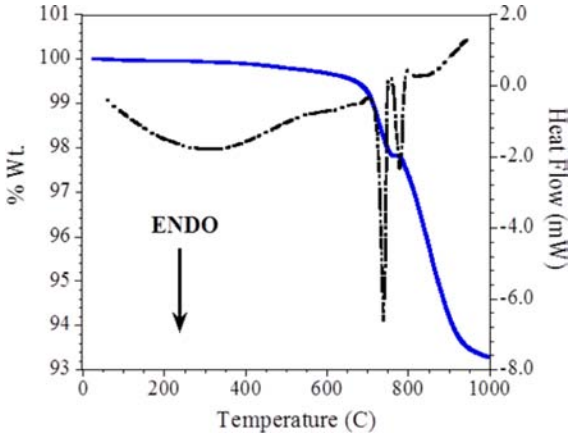

Figure 5. DSC (black curve) and TGA (blue curve) taken on a ground powder of selected crystals of **1**.

evolved species corresponding to the second decomposition because of inconclusive PXRD analysis. Qualitatively, PXRD analysis of **1** shows a gradual loss in crystallinity until the onset of decomposition (as shown by the lower-angle PXRD in Figure S5 in the Supporting Information). A couple of heat treatments including quenching and faster cooling were performed in our follow-up synthesis, and each time the resulting products showed a broadening and intensity reduction of the diffraction peaks. Also, DSC shows negative evidence of an $\alpha \rightarrow \beta$, *Cc* (**1**) to $P4_3$ (**2**), transition. Further studies, including a complete thermal analysis investigating a possible phase transition of $\beta \rightarrow \alpha$, will be carried out upon the availability of a sizable, high-purity sample of **2**.

Final Remarks. Our current study in the exploration of low-dimensional magnetic insulators containing SOJT ions (Bi^{3+}) and magnetic ions ($Mn/Fe^{2+/3+}$) has led to the discovery of three new NCS phases with the formulation of α-$Cs_3KBi_2M_4(PO_4)_6Cl$ (where M = Mn, Fe) for **1** and **3** (*Cc*) and β (where M = Mn) for **2** ($P4_3$). This fascinating family of NCS solids was isolated in reactive molten-salt media, and salt inclusion is evident. The structure adopts by far the most complicated framework among SISs that we have studied thus far. Nonetheless, the discovery of the Cl-centered acentric $Cl(Bi_2Cs)$ unit allows a more explicit structure description in terms of its role as a template to the formation of different polymorphs and, in turn, the corresponding direction of the dipoles. The result of this analysis is expected to be helpful in future structure and property correlation studies.

The unexpected discovery of an exclusive polymorph in Bi_2O_3-rich reactions is worthy of further investigation. The isolation of a single polymorph in the Mn-containing system can possibly be attributed to the change in the "eutectic" melting of the mixed-metal oxides whereby different amounts of Bi_2O_3 were used. However, when "stoichiometric" synthetic attempts were carried out, all evidence pointed to the coexistence of both polymorphs possibly, in part, due to a finite temperature window of formation.

Lastly, these new discoveries suggest that incorporating SOJT ions could initiate another fruitful chapter of salt-inclusion synthesis for new magnetic insulators where the formation of multifunctional NCS solids seems to be promising. It is noted that, like Bi-containing perovskite-like magnetic solids, the components potentially responsible for the occurrence of spontaneous polarization and magnetization are oftentimes physically coupled. To examine that, we will investigate the magnetic susceptibility and ferroelectricity for the possible existence of multiferroic properties in this new series of NCS magnetic solids awaiting the preparation of high-purity sample and/or large-size single crystals.

■ ASSOCIATED CONTENT

Supporting Information

X-ray crystallographic data in CIF format, selected bond distances and angles, BVS calculations, PXRD patterns, and structures. This material is available free of charge via the Internet at http://pubs.acs.org.

■ AUTHOR INFORMATION

Corresponding Author

*E-mail: shwu@clemson.edu.

Notes

The authors declare no competing financial interest.

■ ACKNOWLEDGMENTS

This work has been supported by the National Science Foundation (NSF; Grant DMR-0706426). Support for the purchase of the X-ray diffractometers (Grants ESR-9108772, CHE-9207230, and 9808165) from the NSF is also gratefully acknowledged. We thank Prof. Shiv Halasyamani and Thanh Thao Tran from the University of Houston for SHG measurements of **1**.

■ REFERENCES

(1) (a) Valasek, J. *Phys. Rev.* **1921**, *17*, 475–481. (b) Sawyer, C. B.; Tower, C. H. *Phys. Rev.* **1930**, *35*, 269–273. (c) Franken, P. A.; Hill, A. E.; Peters, C. W.; Weinreich, G. *Phys. Rev. Lett.* **1961**, *7*, 118–119. (d) Chen, C.-T.; Liu, G.-Z. *Annu. Rev. Mater. Sci.* **1986**, *16*, 203–243. (e) Lines, M. E.; Glass, A. M. *Principles and Applications of Ferroelectrics and Related Materials*; Oxford University Press: Oxford, U.K., 1991. (f) Schwartz, R.; Ballato, J.; Haerling, G. *Piezoelectric and Electro-optic Ceramics*; New York, 2004. (g) Ok, K. M.; Chi, E. O.; Halasyamani, P. S. *Chem. Soc. Rev.* **2006**, *35*, 710–717 and references cited therein.

(2) (a) Pearson, R. G. *J. Am. Chem. Soc.* **1969**, *91*, 4947–4955. (b) Stucky, G. D.; Phillips, M. L. F.; Gier, T. E. *Chem. Mater.* **1989**, *1*, 492–509 and references cited therein. (c) Kunz, M.; Brown, I. D. *J. Solid State Chem.* **1995**, *115*, 395–406. (d) Halasyamani, P. S.; Poeppelmeier, K. R. *Chem. Mater.* **1998**, *10*, 2753–2769 and references cited therein. (e) Halasyamani, P. S. *Chem. Mater.* **2004**, *16*, 3586–3592 and references cited therein. (f) Fiebig, M. *J. Phys. D: Appl. Phys.* **2005**, *38*, R123–R152. (g) Mao, J.-G.; Jiang, H.-L.; Kong, F. *Inorg. Chem.* **2008**, *47*, 8498–8510. (h) Sun, C.-F.; Yang, B.-P.; Mao, J.-G. *Sci. China: Chem.* **2011**, *54*, 911–922.

(3) (a) Etheredge, K. M. S.; Hwu, S.-J. *Inorg. Chem.* **1995**, *34*, 3123–3125. (b) Huang, Q.; Hwu, S.-J.; Mo, X. *Angew. Chem., Int. Ed.* **2001**, *40*, 1690–1693. (c) Hwu, S.-J.; Ulutagay-Kartin, M.; Clayhold, J. A.; Mackay, R.; Wardojo, T. A.; O'Connor, C. T.; Krawiec, M. *J. Am. Chem. Soc.* **2002**, *124*, 12404–12405. (d) Clayhold, J. A.; Ulutagay-Kartin, M.; Hwu, S.-J.; Koo, H.-J.; Whangbo, M.-H.; Voigt, A.; Eaiprasertsak, K. *Phys. Rev. B* **2002**, *66*, 052403/1–052403/4. (e) Huang, Q.; Hwu, S.-J. *Inorg. Chem.* **2003**, *42*, 655–657. (f) Mo, X.; Hwu, S.-J. *Inorg. Chem.* **2003**, *42*, 3978–3980. (g) Mo, X.; Ferguson, E.; Hwu, S.-J. *Inorg. Chem.* **2005**, *44*, 3121–3126. (h) Queen, W. L.; West, J. P.; Hwu, S.-J.; VanDerveer, D. G.; Zarzyczny, M. C.; Pavlick, R. A. *Angew. Chem., Int. Ed.* **2008**, *47*, 3791–3794. (i) Queen, W. L.; West, J. P.; Hudson, J.; Hwu, S.-J. *Inorg. Chem.* **2011**, *50*, 11064–11068. (j) Queen, W. L.; West, J. P.; Hwu, S.-J.; Tran, T. T.; Halasyamani, P. S.; VanDerveer, D. *Chem. Commun.* **2012**, *48*, 1665–1667. (k) West, J. P.; Hwu, S.-J. *J. Solid State Chem.* **2012**, http://dx.doi.org/10.1016/j.jssc.2012.06.015.

(4) (a) Wang, S.; Hwu, S.-J. *J. Am. Chem. Soc.* **1992**, *114*, 6920−6922. (b) Wang, S.; Hwu, S.-J.; Paradis, J. A.; Whangbo, M.-H. *J. Am. Chem. Soc.* **1995**, *117*, 5515−5522. (c) Hwu, S.-J. *Chem. Mater.* **1998**, *10*, 2846−2859. (d) Ulutagay-Kartin, M.; Etheredge, K. M. S.; Schimek, G. L.; Hwu, S.-J. *J. Alloys Compd.* **2002**, *338*, 80−86. (e) Queen, W. L.; Hwu, S.-J.; Wang, L. *Angew. Chem., Int. Ed.* **2007**, *46*, 5344−5347. (f) West, J. P.; Hwu, S.-J.; Queen, W. L. *Inorg. Chem.* **2009**, *48*, 8439−8444. (g) West, J. P.; Queen, W. L.; Hwu, S.-J.; Michaux, K. E. *Angew. Chem., Int. Ed.* **2011**, *50*, 3780−3783.

(5) Zhereb, V. P.; Skorikov, V. M. *Inorg. Mater.* **2003**, *39*, S121−S145.

(6) Montanari, E.; Calestani, G.; Migliori, A.; Dapiaggie, M.; Bolzoni, F.; Cabassi, R.; Gilioli, E. *Chem. Mater.* **2005**, *17*, 6457−6467.

(7) Hill, N. A.; Bättig, P.; Daul, C. *J. Chem. Phys. B* **2002**, *106*, 3383−3388.

(8) Hill, N. A.; Rabe, K. M. *Phys. Rev. B* **1999**, *59*, 8759−8769.

(9) (a) Kizelev, S. V.; Ozerov, R. P.; Zhdanov, G. S. *Sov. Phys. Dokl.* **1962**, *145*, 1255. (b) Kubel, F.; Schmid, H. *Acta. Crystallogr., Sect. B* **1990**, *46*, 698.

(10) Hill, N. A.; Filippetti, A. *J. Magn. Magn. Mater.* **2002**, *242−245*, 976−979.

(11) Huang, Q.; Ulutagay, M.; Hwu, S.-J. *J. Am. Chem. Soc.* **1999**, *121*, 10323−10326.

(12) Ketatni, M.; Mentre, O.; Abraham, F.; Kzaiber, K.; Mernari, B. *J. Solid State Chem.* **1998**, *139*, 274−280.

(13) Jacobson, R. A. *REQAB Empirical Absorption Correction*, version 1.1-03101998; Molecular Structure Corp.: Research Forest, TX, 1996−1998.

(14) *CrystalClear*; Rigaku/MSC: The Woodland, TX, 1999.

(15) (a) Sheldrick, G. M. In *Crystallographic Computing 3*; Sheldrick, G. M., Kruger, C., Goddard, R., Eds.; Oxford University Press: London, 1985; pp 175−189. (b) Sheldrick, G. M. *SHELXTL, Structure Determination Software Programs*, version 6.1; Bruker Analytical X-ray Systems Inc.: Madison, WI, 2001.

(16) (a) Spek, A. L. *Acta Crystallogr.* **1990**, *A46*, C-34. (b) Spek, A. L. *A Multipurpose Crystallographic Tool*; Utrecht University: Utrecht, The Netherlands, 2002.

(17) *CRC Handbook of Chemistry and Physics*, 87th ed.; CRC Press: Boca Raton, FL, 2006−2007.

(18) West, A. R. *Solid State Chemistry and Its Applications*; John Wiley & Sons: New York, 1996; p 314.

(19) Shannon, R. D. *Acta Crystallogr.* **1976**, *A32*, 751−767.

(20) Brese, N. E.; O'Keefe, M. *Acta Crystallogr.* **1991**, *B47*, 192−197.